nature immunology

Caveolin-1-dependent nanoscale organization of the BCR regulates B cell tolerance

Susana Minguet[1–4], Kathrin Kläsener[1,2,5], Anna-Maria Schaffer[1,3], Gina J Fiala[1,2], Teresa Osteso-Ibánez[4], Katrin Raute[1,2,6], Inmaculada Navarro-Lérida[4], Frederike A Hartl[1,2], Maximilian Seidl[3,7], Michael Reth[1,2,5] & Miguel A Del Pozo[4]

Caveolin-1 (Cav1) regulates the nanoscale organization and compartmentalization of the plasma membrane. Here we found that Cav1 controlled the distribution of nanoclusters of isotype-specific B cell antigen receptors (BCRs) on the surface of B cells. In mature B cells stimulated with antigen, the immunoglobulin M BCR (IgM-BCR) gained access to lipid domains enriched for GM1 glycolipids, by a process that was dependent on the phosphorylation of Cav1 by the Src family of kinases. Antigen-induced reorganization of nanoclusters of IgM-BCRs and IgD-BCRs regulated BCR signaling *in vivo*. In immature Cav1-deficient B cells, altered nanoscale organization of IgM-BCRs resulted in a failure of receptor editing and a skewed repertoire of B cells expressing immunoglobulin-μ heavy chains with hallmarks of poly- and auto-reactivity, which ultimately led to autoimmunity in mice. Thus, Cav1 emerges as a cell-intrinsic regulator that prevents B cell–induced autoimmunity by means of its role in plasma-membrane organization.

The B cell antigen receptor (BCR) is a multiprotein complex expressed on the surface of B cells that transmits critical signals for the development, proliferation and activation of B cells. The BCR consists of two identical immunoglobulin heavy chains (HCs) and two identical light chains (LCs) that form the antigen-binding molecule, which is associated with the signal-transduction unit composed of a heterodimer of the immunoglobulin α-chain (CD79a) and immunoglobulin β-chain (CD79b)[1]. Signaling from the BCR is triggered by the engagement of ligands and leads to activation of the B cell. The BCR lacks intrinsic tyrosine-kinase activity, but signaling is achieved by phosphorylation of its immunoreceptor tyrosine-based activation motifs (ITAMs)[2] by the tyrosine kinases Lyn (a member of the Src family) and Syk[3]. The recruitment of Syk to phosphorylated ITAMs amplifies signal transduction via the BCR[4].

BCR signaling ensures the generation of a naive antibody repertoire from which autoreactive specificities have been removed[5]. During early B cell development in the bone marrow (BM), gene segments encoding the immunoglobulin variable regions are stochastically recombined, which generates an enormous diversity of antibody specificities (1×10^{11})[6,7]. This process can generate BCRs that recognize the body's self components and potentially leads to autoimmunity. For silencing of those autoreactive BCRs, central tolerance is established by mechanisms such as deletion, anergy and receptor editing[8,9]. It has been estimated that 25–50% of the naturally arising antibodies in mice undergo receptor editing by LC replacement[10,11]. In humans, up to 75% of the newly generated antibodies are potentially self-reactive but are efficiently removed during B cell development[12]. Diminished BCR signaling impairs the counter-selection of autoreactive B cells by failing to induce tolerance mechanisms in immature B cells in mice and humans[13–15].

Immature B cells exclusively express immunoglobulin M BCRs (IgM-BCRs), whereas mature B cells co-express both IgM-BCRs and IgD-BCRs of identical antigen specificity. Both IgM-BCRs and IgD-BCRs form nanoclusters on the surface of resting B cells ('protein islands')[16–20]. The IgM-BCRs and IgD-BCRs reside in different class-specific membrane compartments with distinct compositions of protein and lipid[18–20]. The IgD compartment shows enrichment for ordered lipid domains, while the IgM-BCR gains access to such lipids only after the activation of B cells. Published reports suggest that nanoclustering of BCRs is important for shaping BCR signaling[18,20]. So far, little is known about how such membrane organization is regulated at the molecular level.

Caveolin-1 (Cav1) is a membrane protein that promotes the assembly and stability of ordered lipid domains in several cell types[21]. In addition, Cav1 modulates the assembly and activity of multimolecular signaling complexes through interactions with its phosphorylated

[1]Department of Immunology, Institute for Biology III, Faculty of Biology, University of Freiburg, Freiburg, Germany. [2]Centre for Biological Signalling Studies BIOSS, University of Freiburg, Freiburg, Germany. [3]Center for Chronic Immunodeficiency (CCI), University Medical Center Freiburg, Faculty of Medicine, University of Freiburg, Freiburg, Germany. [4]Mechanoadaptation & Caveolae Biology Lab, Cell Biology & Physiology Program; Cell & Developmental Biology Area, Centro Nacional de Investigaciones Cardiovasculares Carlos III (CNIC), Madrid, Spain. [5]Max Planck Institute of Immunology and Epigenetics, Freiburg, Germany. [6]Spemann Graduate School for Biology and Medicine (SGBM), University of Freiburg, Freiburg, Germany. [7]Institute for Surgical Pathology, University Medical Center Freiburg, University of Freiburg, Freiburg, Germany. Correspondence should be addressed to S.M. (susana.minguet@biologie.uni-freiburg.de).

Received 11 May; accepted 11 July; published online 14 August 2017; doi:10.1038/ni.3813

Tyr14 residue or its scaffolding domain[21,22]. Increased lipid mobility, an enhanced abundance of ordered domains and accelerated endocytosis have been reported in cells lacking Cav1 expression[23–25]. It was initially reported that lymphocytes do not express Cav1, on the basis of the analysis of several B cell and T cell lines[26]. However, subsequent studies have proven a role for Cav1 in primary T cells[27,28]. Furthermore, Cav1 has been detected in splenic B cells stimulated with lipopolysaccharide (LPS), and is seems to have a role in T cell–independent antibody responses *in vivo*[29].

Given the role of Cav1 in membrane compartmentalization, we hypothesized that Cav1 regulates the nanoscale distribution IgM-BCRs and IgD-BCRs on the surface of B cells. Our results showed that the IgM-BCR gained access to domains enriched for GM1 glycolipids after triggering of the BCR by a process that was regulated by the phosphorylation of Cav1 by kinases of the Src family. Accordingly, the activation of mature *Cav1*$^{-/-}$ B cells *in vivo* and *ex vivo* was impaired, and *Cav1*$^{-/-}$ immature B cells showed diminished receptor editing, which resulted in a skewed BCR repertoire of immunoglobulin-μ HCs (μHCs) with hallmarks of poly- and auto-reactivity. Correspondingly, *Cav1*$^{-/-}$ mice exhibited splenomegaly, high titers of serum autoantibodies, spontaneous formation of germinal centers (GC) and a shortened lifespan.

RESULTS

Cav1 regulates nanoclustering of IgM-BCRs

Primary B cells expressed Cav1 (**Supplementary Fig. 1a**). Therefore, we investigated whether Cav1 regulates the nanoscale organization of IgM-BCRs and IgD-BCRs on the surface of B cells. We performed an *in situ* proximity-ligation assay (PLA) with non-permeabilized primary B cells from C57BL/6 wild-type mice (B6.WT) and C57BL/6 mice deficient in Cav1 (B6.Cav1KO mice)[30] to quantify the proximity of the BCR to the cholera toxin B subunit (CTxB) on the B cell surface (**Supplementary Fig. 1b**). CTxB binds with high affinity to GM1 glycolipids, for which cholesterol- and sphingolipid-rich membrane domains show enrichment ('ordered lipid domains')[31]. The control samples were resting or pervanadate (perV)-stimulated primary B cells (**Supplementary Fig. 1c**). As reported[18], in resting wild-type splenic B cells, the IgM-BCR was mainly excluded from GM1-enriched domains (**Fig. 1a**). However, in resting Cav1-deficient B cells (from B6.Cav1KO mice), a significant proportion of IgM-BCRs were found in close proximity to GM1 (**Fig. 1a**). On the surface of wild-type B cells, the proximity of the IgM-BCR to GM1-enriched lipid domains reached a maximum at 5 min after triggering of the BCR and decreased to basal levels after 20 min, probably due to the internalization of BCRs (**Supplementary Fig. 1d**). On Cav1-deficient B cells, the already close proximity of IgM-BCR to GM1 remained unchanged after stimulation either with antibody to the BCR (anti-BCR) or with perV (**Fig. 1a**). Cav1 was next expressed in the Cav1-deficient mouse B cell line K46 in a gain-of-function approach (**Supplementary Fig. 1e**,**f**). Again, the IgM-BCR gained access to GM1-enriched lipid domains upon B cell activation only in K46 cells expressing Cav1, as noted by PLA (**Supplementary Fig. 1e**) and by purification of detergent-resistant membranes (DRMs) (**Supplementary Fig. 1f**). Lack of Cav1 did not globally disrupt membrane topology, since the basal amount of DRM-associated molecules, such as GM1 and LYN, was similar in cells expressing Cav1 or a Cav1 mutant that cannot be phosphorylated and in cells lacking Cav1 expression (**Supplementary Fig. 1f**). BCR-induced translocation of the actin-remodeling GTPase Rac1 to DRMs, which is required for its activation, occurred only in the presence of Cav1 (**Supplementary Fig. 1f**), which suggested defective BCR-induced signaling in Cav1-deficient B cells. Thus, Cav1 regulated the nanoscale distribution of the IgM-BCR both in the resting state and after stimulation of the BCR.

Phosphorylation of Cav1 regulates BCR nanoclustering

We next investigated the role of the Src family of kinases in the reorganization of IgM-BCRs after activation of the BCR by incubating primary B cells with the Src-kinase inhibitor PP2. Translocation of the IgM-BCR to GM1-enriched lipid domains in *Cav1*$^{+/+}$ B cells was significantly blocked in the presence of PP2, comparable to the blockade seen in their Cav1-deficient counterparts (**Fig. 1b**). The Src family of kinases has been reported to phosphorylate both the BCR[32] and Cav1 at Tyr14 (ref. 33). To clarify whether phosphorylation of Cav1 regulates the membrane compartmentalization of IgM-BCR, we purified B cells from mice expressing mutant Cav1 that cannot be phosphorylated (C57BL/6 *Cav1*$^{Y14F/Y14F}$ mice; called 'B6.Cav1$^{Y14F/Y14F}$' here)[28]. Both the steady-state distribution of the IgM-BCR, relative to GM1-enriched lipid domains, and its activation-induced distribution were modulated by phosphorylation of Cav1 at Tyr14 (**Fig. 1c**). IgM-BCRs and IgD-BCRs are found in separated class-specific compartments in wild-type B cells that coalesce only after B cell stimulation[34]. The proportion of IgD-BCRs near GM1-enriched lipid domains was significantly lower in resting B6.Cav1KO splenic B cells than in resting wild-type splenic B cells (**Fig. 1d**). Stimulation of the BCR reduced the proximity of the IgD-BCR to GM1-enriched lipid domains in wild-type B cells but not in B6.Cav1KO or B6.Cav1$^{Y14F/Y14F}$ B cells (**Fig. 1d**), which indicated that the activation-induced distribution of IgD-BCRs was regulated by phosphorylation of Cav1 at Tyr14. The steady-state class-specific separation of the IgM-BCR nanoclusters from the IgD-BCR nanoclusters was perturbed both in B6.Cav1KO B cells and B6.Cav1$^{Y14F/Y14F}$ B cells (**Fig. 1e**). After stimulation of the BCR, the coalescence of IgM-BCRs and IgD-BCRs was diminished in B6.Cav1$^{Y14F/Y14F}$ B cells and was abolished in B6.Cav1KO B cells (**Fig. 1e**). Notably, the steady-state surface expression of the IgM-BCR and IgD-BCR and the BCR-internalization kinetics were indistinguishable in wild-type B cells, B6.Cav1KO B cells and B6.Cav1$^{Y14F/Y14F}$ B cells (**Supplementary Fig. 2a**,**b**). Thus, phosphorylation of Cav1 at Tyr14 was required for the steady-state separation of IgM-BCRs from IgD-BCRs and for the optimal reorganization of both BCR isotypes after stimulation.

The BCR gains proximity to Cav1 after B cell activation

Next we used *in situ* PLA to investigate whether the cytoplasmic part of the BCR (the immunoglobulin α-chain) also gained proximity to Cav1 after triggering of the BCR in permeabilized cells (**Supplementary Fig. 2c**,**d**). In resting primary B cells, the cytoplasmic part of the BCR and Cav1 were >40 nm apart, as no PLA signal was detected (**Fig. 2**). After activation of B cells, the BCR and Cav1 gained proximity to each other gradually for the first 15 min after stimulation (**Fig. 2**). This proximity was induced by treatment with anti-IgM or perV but was independent of the phosphorylation of Cav1 at Tyr14 (**Fig. 2**). Similar results were obtained with K46 cells expressing Cav1 (**Supplementary Fig. 2e**). Thus, the activation of B cells was accompanied by greater proximity between the cytoplasmic regions of the BCR and Cav1, and this reorganization did not require phosphorylation of Cav1 at Tyr14. These results were compatible with lateral reorganization of the BCR within the plasma membrane and with conformational changes in the immunoglobulin α-chain cytoplasmic tail[35].

Diminished B cell activation in mice lacking Cav1

Our results showed that in the absence of Cav1, the nanodistribution of the IgM-BCRs and IgD-BCRs was altered. To investigate the

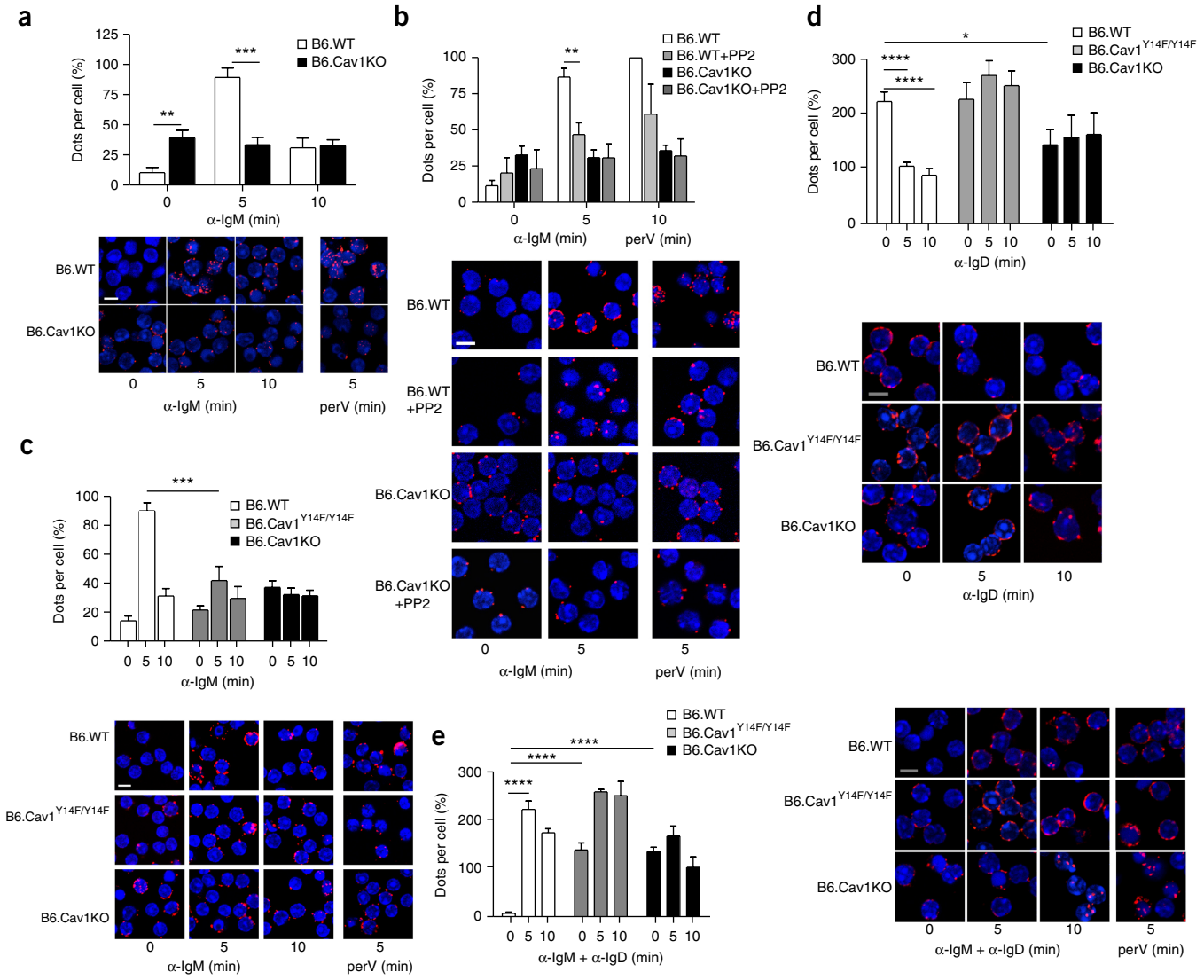

Figure 1 Cav1 regulates the nanoclustering of IgM-BCRs and IgD-BCRs. (**a**) PLA (top) of purified splenic B6.WT or B6.Cav1KO B cells (key) left unstimulated (0) or stimulated for 5 or 10 min (horizontal axis) with anti-IgM F(ab′)$_2$ (α-IgM) (10 μg/ml), assessing the proximity of the IgM-BCR to GM1; results were normalized to those of B6.WT cells stimulated for 5 min with perV (0.5 mM). Below, microscopy of cells as in the analysis above, showing nuclei stained with the DNA-binding dye DAPI (blue) and PLA signals (red). (**b**) PLA (top) and microscopy (bottom) of purified splenic B6.WT or B6.Cav1KO B cells pretreated for 60 min with vehicle or 10 μM PP2 (+ PP2) (key), then stimulated and analyzed as in **a**. (**c**) PLA (top) and microscopy (bottom) of purified splenic B6.WT, B6.Cav1$^{Y14F/Y14F}$ or B6.Cav1KO B cells (key) stimulated and analyzed as in **a**. $P = 0.004$, unstimulated B6.Cav1$^{Y14F/Y14F}$ and B6.Cav1KO versus B6.WT (analysis of variance (ANOVA)). (**d**) PLA (top) of purified splenic B cells left unstimulated (0) or stimulated for 5 or 10 min (horizontal axis) with anti-IgD F(ab′)$_2$ (10 μg/ml), assessing the proximity of the IgD-BCR to GM1. Below, microscopy as in **a**. $P = 0.05$, unstimulated B6.Cav1$^{Y14F/Y14F}$ and B6.Cav1KO versus B6.WT (ANOVA). (**e**) PLA (left) of purified splenic B cells left unstimulated (0) or stimulated for 5 or 10 min (horizontal axis) with anti-IgM F(ab′)$_2$ (10 μg/ml) plus anti-IgD F(ab′)$_2$ (10 μg/ml), assessing the proximity of the IgM-BCR to the IgD-BCR. Right, microscopy as in **a**. $P < 0.0001$, unstimulated B6.Cav1$^{Y14F/Y14F}$ and B6.Cav1KO versus B6.WT (ANOVA). Scale bars, 5 μm. $^*P \le 0.05$, $^{**}P \le 0.01$, $^{***}P \le 0.001$ and $^{****}P \le 0.0001$ (unpaired Student's *t*-test (comparison of only two conditions) or ANOVA followed by Dunnett's multiple-comparisons test). Data are pooled from at least three experiments with at least 300 cells per condition in each (mean + s.e.m.).

implications for B cell activation *in vivo*, we used two Cav1-deficient models that differ in the *Cav1* exon disrupted and their genetic background: disruption of exon 3 on the C57BL/6 background (B6.Cav1KO)[30], or disruption of exon 2 on a mixed background (129/Sv, C57BL/6J and SJL; called 'Cav1KO' here)[36]. B6.Cav1KO and Cav1KO mice were immunized with the T cell–independent antigen nitrophenol (NP)-Ficoll, precipitated with alum. The proportion of antigen-specific B cells was significantly lower in the spleen of both Cav1-deficient models than in their wild-type counterparts (**Fig. 3a**,**b** and **Supplementary Fig. 3a**,**b**). Furthermore, the clonal expansion of splenic B cells, as measured by staining of the proliferation marker Ki67, was also lower in both Cav1-deficient models than in their wild-type counterparts (**Fig. 3c** and **Supplementary Fig. 3c**). The abundance of NP-specific antibody-secreting cells and NP-specific serum antibodies was significantly also lower in both Cav1-deficient models than in their wild-type counterparts (**Fig. 3d**,**e**). In agreement with a published report[29], no differences were observed for T cell–dependent responses (data not shown).

To address whether impaired BCR-induced signaling was responsible for the diminished *in vivo* responses, we performed *ex vivo* stimulation of splenic B cells. First, BCR-induced proliferation was lower in both Cav1-deficient models than in their wild-type counterparts, whereas stimulation with LPS resulted in substantial proliferation in both Cav1-deficient models equivalent to that in their wild-type counterparts (**Fig. 3f** and **Supplementary Fig. 3d**), which indicated that signaling from the BCR was specifically affected. Second, B cells from both Cav1-deficient models showed lower BCR-induced expression of the early activation markers CD69 and CD86 than that of their wild-type counterparts (**Fig. 3g**,**h** and **Supplementary Fig. 3e**). Third, calcium-flux responses after triggering of BCR were diminished in primary cells lacking Cav1 in both models, relative to the responses in their wild-type counterparts (**Fig. 3i** and **Supplementary Fig. 3f**). Finally, phosphorylation of Syk, which is crucial for signal transduction from the BCR, was lower in Cav1-deficient B cells than in wild-type cells (**Fig. 3j**). B6.Cav1$^{Y14F/Y14F}$ B cells exhibited a less altered phenotype in terms of BCR-induced signaling (**Fig. 3g**,**h**,**j**). Hence, the activation of B cells was diminished both *in vivo* and *ex vivo* in the absence of Cav1, as shown by two independent mouse models of Cav1 deficiency.

Aged Cav1-deficient mice develop features of autoimmunity

Cav1-deficient mice have a shortened lifespan that has been attributed to secondary complications such as pulmonary fibrosis, hypertension or cardiac hypertrophy[37]. We confirmed those data (**Supplementary Fig. 4a**) and extended the findings to the B6.Cav1KO model (**Fig. 4a**). Mutant mice of both models (B6.Cav1KO and Cav1KO) exhibited large spleens, which were detectable from 15 weeks of age onward and became more obvious in aged mice (>30 weeks of age) (**Fig. 4b** and **Supplementary Fig. 4b**,**c**). Both the total number of B cells and the proportion of B cells in the spleen were significantly greater in Cav1-deficient mice than in their wild-type counterparts (**Fig. 4c**,**d** and **Supplementary Fig. 4d**). For aged mice, the abundance of spontaneously generated GCs and class-switched B cells was significantly greater in Cav1-deficient mice than in their wild-type counterparts (**Fig. 4e**,**f** and **Supplementary Fig. 4e**,**f**). Proliferating Ki67$^+$ B cells formed morphological structures that resembled clonally expanding B cells in the spleen of aged mice (**Supplementary Fig. 4g**). The abundance of IgG immunocomplexes in the kidneys was greater in aged Cav1-deficient mice than in their age-matched wild-type counterparts (**Fig. 4g** and **Supplementary Fig. 4i**,**j**). Aged Cav1-deficient mice had significantly higher serum titers of spontaneously generated anti-cardiolipin and IgG autoantibodies to double-stranded DNA (dsDNA) than those of their aged-matched wild-type counterparts, while their concentration of total IgG was similar to that of their age-matched wild-type counterparts (**Fig. 4h** and **Supplementary Fig. 4h**). No significant abnormalities were found in the myeloid or T cell lineages (data not shown). Thus, aged Cav1-deficient mice developed features of immunological dysregulation characterized by spontaneous GC formation, an increased number of B cells in the spleen, elevated titers of serum autoantibodies and shorter lifespan.

B cell–specific autoimmunity in Cav1-deficient mice

Our data showed immunological dysregulation in two mouse models of Cav1 deficiency. We next generated BM chimeras to investigate the contribution of B cells to this phenotype. First, sublethally irradiated immunodeficient *Rag2*$^{-/-}$*Il2rg*$^{-/-}$ mice (called '*Rag2*$^{-/-}\gamma c^{-/-}$ mice' here) reconstituted with Cav1KO BM showed a significantly shorter lifespan than that of their counterparts reconstituted with wild-type BM ($P = 0.04$; **Supplementary Fig. 5a**,**b**), which proved

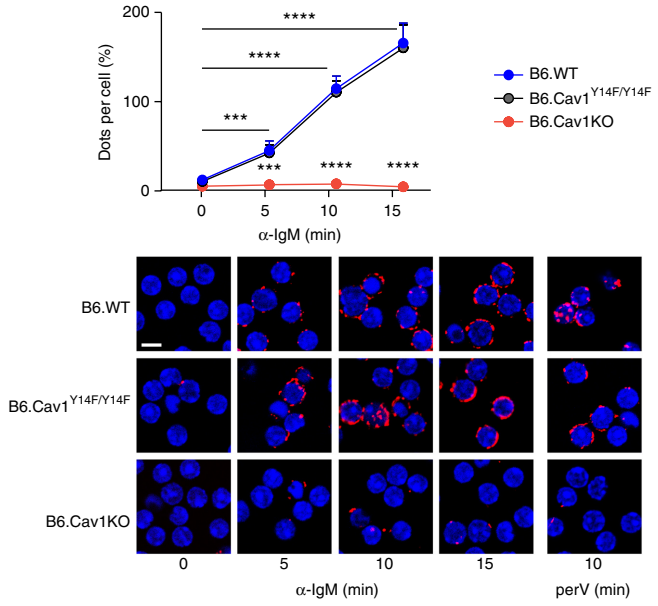

Figure 2 Cav1 and the BCR reach close proximity after BCR stimulation. PLA (top) of purified splenic B6.WT, B6.Cav1$^{Y14F/Y14F}$ or B6.Cav1KO B cells (key) left unstimulated (0) or stimulated for 5, 10 or 15 min (horizontal axis) with anti-IgM F(ab′)$_2$ (10 μg/ml), then fixed, permeabilized and assessed *in situ* for the proximity of the immunoglobulin α-chain cytoplasmic tail to Cav1; results were normalized to those of perV-stimulated B6.WT cells. Below, microscopy of cells as in the analysis above (assessed as in **Fig. 1a**). Scale bar, 5 μm. *P* values, resting versus stimulated (B6.WT) or B6.WT versus B6.Cav1KO (Student's *t*-test). $^{***}P \leq 0.001$ and $^{****}P \leq 0.01$ (ANOVA). Data are pooled from five experiments with at least 300 cells per condition in each (mean + s.e.m.).

that the shorter lifespan previously reported for *Cav1*$^{-/-}$ mice[37] resulted from their dysregulated immune system. After 25 weeks, the surviving mice were killed and analyzed. The spleen of chimeras reconstituted with Cav1KO cells showed significantly enlargement ($P = 0.01$; **Supplementary Fig. 5c**), and the frequency of spontaneously generated GC B cells was greater ($P = 0.06$; **Supplementary Fig. 5d**), relative to that of their counterparts in mice reconstituted with wild-type cells. Significantly higher titers of IgG antibodies to cardiolipin ($P = 0.005$) and to dsDNA ($P = 0.05$) were detected in mice reconstituted with Cav1KO cells than in those reconstituted with wild-type cells (**Supplementary Fig. 5e**). Hence, the immunological dysregulation in Cav1-deficient mice had its origin in their immune system.

We performed competitive BM reconstitution to confirm those findings and to narrow down the population responsible for that phenotype. *Rag2*$^{-/-}\gamma c^{-/-}$ mice were reconstituted with B6.Cav1KO BM cells or C57BL/6 wild-type (B6.WT) BM cells (each expressing the congenic marker CD45.2) together with wild-type BM cells (expressing CD45.1; CD45.1WT) at a cell ratio of 1:1. In the B6.Cav1KO–CD45.1WT chimeras, 73% ± 3% (mean ± s.e.m.) of the B cells in the BM were Cav1-deficient (B6.Cav1KO) cells (**Fig. 5a**). Significant accumulation of Cav1-deficient B cells was detected from the immature B cell stage onward (**Fig. 5b**). Similarly, Cav1-deficient cells constituted 71% ± 2% of splenic lymphocytes, whereas wild-type cells accounted for the expected 49% ± 0.6% of splenocytes, in the B6.WT–CD45.1WT chimeras (**Fig. 5c**,**d**). In the peripheral lymph nodes, Cav1-deficient B cell populations were also specifically expanded (**Fig. 5e**), whereas

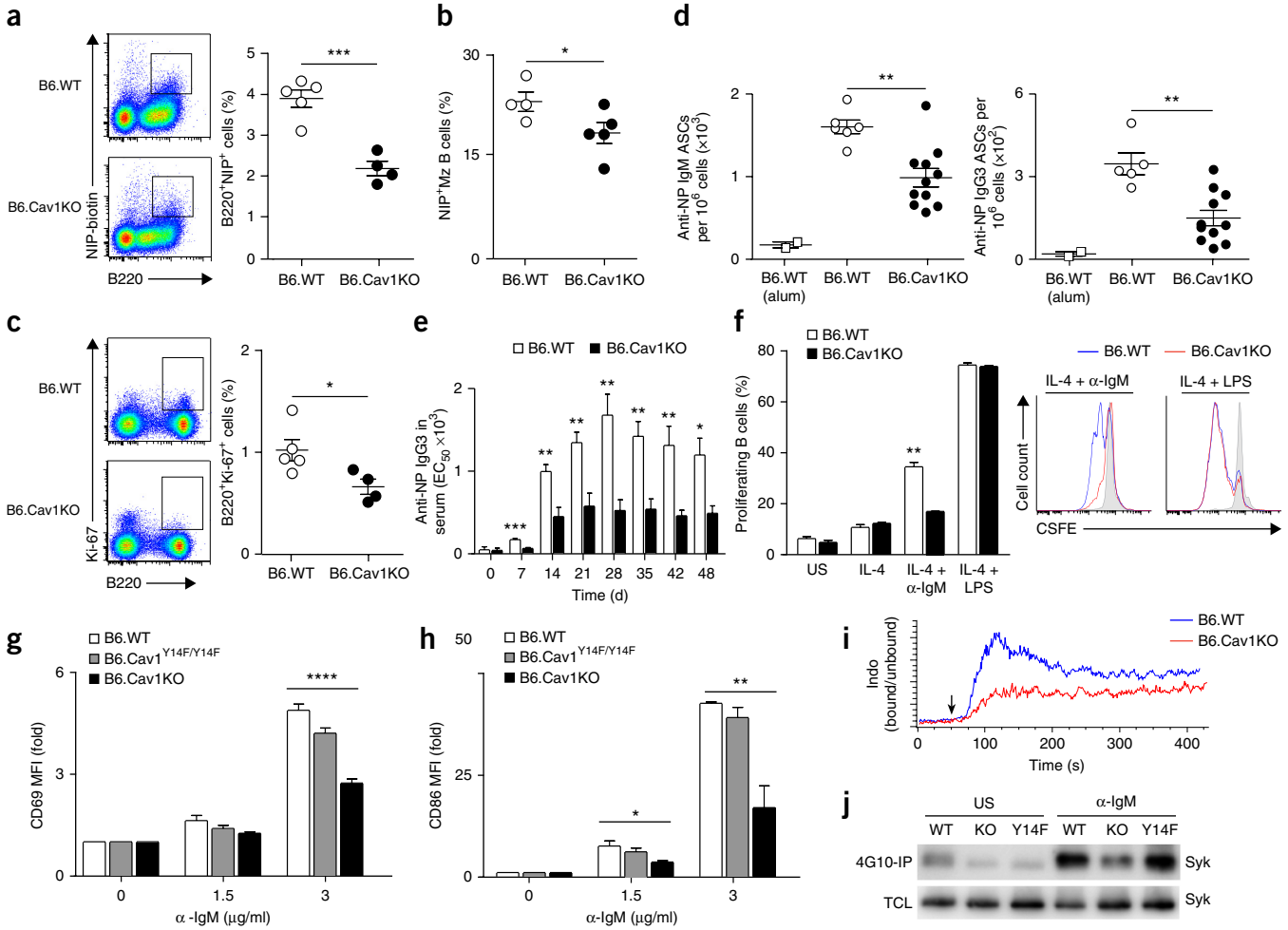

Figure 3 The absence of Cav1 diminishes B cell responses in B6.Cav1KO mice. (**a**) Flow cytometry of splenocytes from B6.WT and B6.Cav1KO mice immunized with alum-precipitated NP-Ficoll, assessing staining with the biotin-conjugated hapten NIP and anti-B220 (left) to define the frequency of NP-reactive (NIP^+) B cells ($B220^+$) among splenocytes (right). (**b**,**c**) Frequency of NP-reactive B cells in the splenic marginal zone (MZ) (**b**), and flow cytometry assessing staining with Ki67 and anti-B220 (left) and frequency of proliferating ($Ki67^+$) B cells (right) (**c**) in mice as in **a**. (**d**) ELISPOT analysis of splenic NP-specific IgM-secreting cells (left) and NP-specific IgG3-secreting cells (right) in mice 7 d after immunization with alum-precipitated NP-Ficoll, or with alum only (far left: B6.WT mice; control). ASC, antibody-secreting cell. (**e**) ELISA of NP-specific IgG3 in serial dilutions of serum from mice immunized with NP-Ficoll; results are presented as the half-maximum effective concentration (EC_{50}). (**f**) Proliferation of splenic B cells labeled with the division-tracking dye CFSE and left unstimulated (US (left) or gray shaded curve (right)) or stimulated for 3 d with IL-4 (50 ng/ml) alone or in combination with anti-IgM $F(ab')_2$ (3 μg/ml) or LPS (1 μg/ml) (above or below plots), assessed by flow cytometry as dilution of CFSE. (**g**,**h**) Flow cytometry analyzing the expression of CD69 (**g**) or CD86 (**h**) by splenic B cells purified from B6.WT, B6.$Cav1^{Y14F/Y14F}$ or B6.Cav1KO mice (key) and stimulated for 18 h with various concentrations (horizontal axis) of anti-IgM $F(ab')_2$; results are presented as mean fluorescence intensity (MFI) relative to that of unstimulated cells, set as 1. $^*P = 0.04$, $^{**}P = 0.003$ and $^{****}P \leq 0.0001$, B.$Cav1^{Y14F/Y14F}$ and B6.Cav1KO versus B6.WT (ANOVA followed by Dunnett's multiple-comparisons test (bracketed)). (**i**) Calcium flux in B6.WT and B6.Cav1KO cells (key), assessed by flow cytometry at baseline (acquired for 50 s) and then after the addition (downward arrow) of anti-IgM $F(ab')_2$ (8 μg/ml) and presented as the ratio of Ca^{2+}-bound Indo (fluorescent Ca^{2+} indicator dye) to Ca^{2+}-unbound Indo. (**j**) Immunoblot analysis of Syk in lysates of purified B6.WT (WT), B6.Cav1KO (KO) or B6.$Cav1^{Y14F/Y14F}$ (Y14F) B cells (above lanes) left unstimulated or stimulated for 5 min with anti-IgM $F(ab')_2$ (10 μg/ml) (above blots), assessed in an aliquot of the total cellular lysate (TCL) or after incubation overnight with 4G10-coupled beads (for immunoprecipitation (IP) of phosphorylated tyrosine) (4G10-IP) (left margin). Each symbol (**a**–**d**) represents an individual mouse ($n = 4$–5 per group in **a**-**c**; $n = 6$–11 mice per group in **d**); small horizontal lines indicate the mean (± s.e.m.). $^*P \leq 0.05$, $^{**}P \leq 0.01$ and $^{***}P \leq 0.001$ (unpaired Student's *t*-test (except where stated otherwise); presented as in **Fig. 1**). Data are representative of two independent experiments (**a**–**c**,**f**,**i**; mean + s.e.m. in **f**), or three independent experiments (**j**) or are pooled from two independent experiments (**d**,**e**,**g**,**h**; mean + s.e.m. in **g**,**h**).

the proportion of various T cell populations conserved the 1:1 ratio in in the spleen, lymph nodes and thymus of both chimeras (**Fig. 5f** and **Supplementary Fig. 5f**–**i**). When spontaneously formed GC B cells were analyzed, up to 73% ± 6% of them lacked Cav1 expression in the B6.Cav1KO-CD45.1WT chimera (**Fig. 5g**). Moreover, the B6.Cav1KO–CD45.1WT chimeras exhibited higher titers of serum autoantibodies than did the B6.WT–CD45.1WT chimeras (**Fig. 5h**).

Finally, $Rag2^{-/-}\gamma c^{-/-}$ mice were reconstituted with BM cells from B6.$Cd79a^{-/-}$ mice (C57BL/6 mice that are deficient in the immunoglobulin α-chain (CD79a) and therefore lack B cells) and either B6.Cav1KO BM cells or B6.WT BM cells at a cell ratio of 1:1. In this experimental setup, Cav1-deficient B cells do not compete with wild-type B cells but reconstitute recipient mice together with Cav1-expressing cells of the other hematopoietic lineages. The lifespan of mice reconstituted with B6.Cav1KO BM cells was significantly

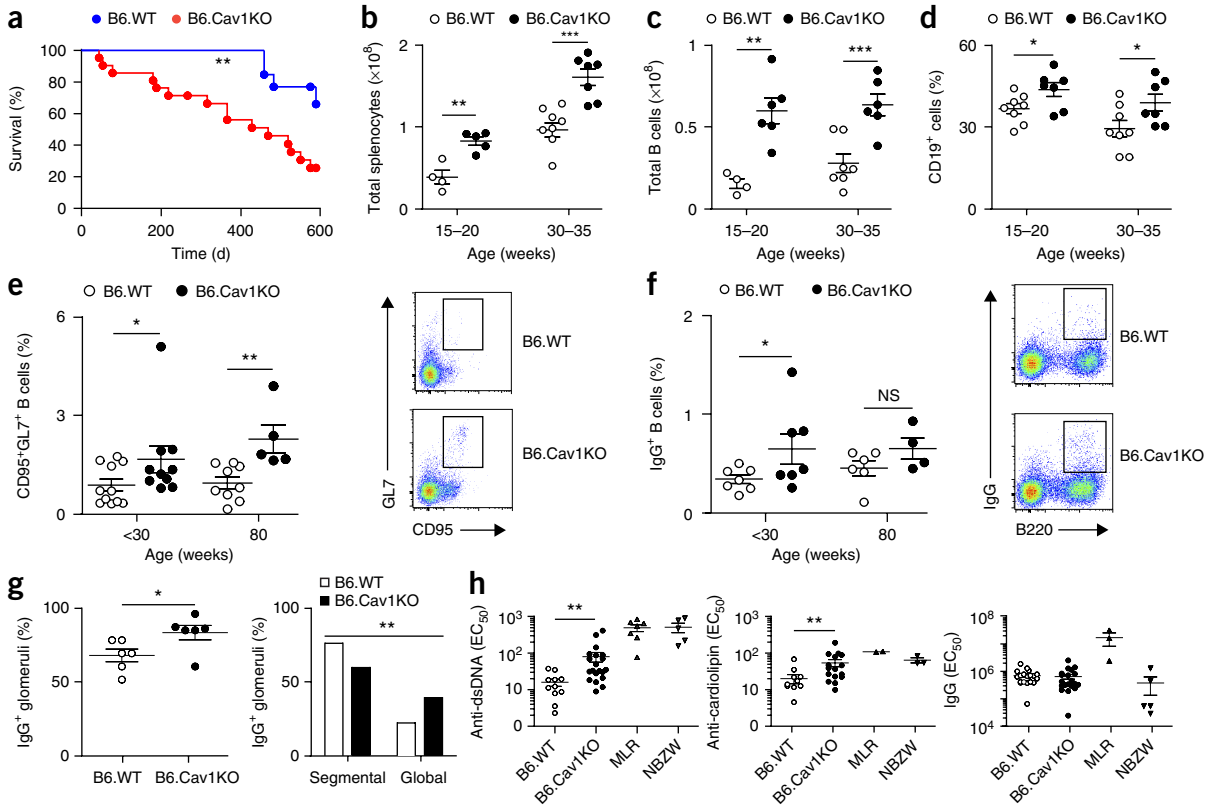

Figure 4 B6.Cav1KO mice have a greater number of B cells, spontaneous GC formation, autoantibodies and shorter lifespan. (**a**) Survival of B6.WT and B6.Cav1KO mice (key; $n = 60$ per genotype). *P* value, log-rank (Mantel-Cox) test. (**b**) Total splenocytes in adult (15–20 weeks of age) and aged (30–35 weeks of age) B6.WT and B6.Cav1KO mice. (**c**,**d**) Total B cells (**c**) and proportion of B cells (CD19$^+$) (**d**) in the spleen of adult and aged mice (as in **b**). (**e**) Frequency of GC (CD95$^+$GL7$^+$) B cells in the spleen of untreated mice (<30 weeks of age) and very old mice (80 weeks of age) (left), gated as at right. (**f**) Frequency of class-switched IgG1$^+$ B cells in the spleen of mice as in **e** (left), gated as at right. (**g**) Frequency of glomeruli with IgG deposits in the kidneys of 80-week-old mice (left), and segmental (<50%) or global (>50%) distribution of IgG in IgG$^+$ glomeruli in those mice (right). $^{**}P = 0.009$, χ^2 contingency analysis. (**h**) ELISA of anti-dsDNA (left), anti-cardiolipin (middle) and total IgG (right) in serial dilutions of serum from old (50–80 weeks of age) B6.WT and B6.Cav1KO mice, as well as autoimmune MLR/lpr (MLR) and NBZW mice (positive control) (presented as in **Fig. 3e**). Kolmogorov-Smirnov test (normal data distribution); *P* values, Mann-Whitney test. Each symbol (**b**–**h**) represents an individual mouse ($n = 4$–8 per group (**b**); $n = 4$–7 per group (**c**); $n = 7$–8 per group (**d**); $n = 5$–11 per group (**e**); $n = 4$–7 per group (**f**); $n = 6$–8 per group (**g**); and $n = 11$–20 per group (**h**)); small horizontal lines indicate the mean (± s.e.m.). $^*P \leq 0.05$, $^{**}P \leq 0.01$ and $^{***}P \leq 0.001$ (Student's *t*-test (except where stated otherwise); presented as in **Fig. 1**). Data are representative of 60 experiments (**a**) or 4–20 experiments (**b**–**h**), with one mouse in each.

shorter than that of mice reconstituted with B6.WT BM (**Fig. 5i**). The surviving mice reconstituted with B6.*Cd79a*$^{-/-}$ BM plus B6.Cav1KO BM had a specifically expanded B cell compartment in the spleen (**Fig. 5j**) and elevated serum IgG autoantibodies directed against cardiolipin (**Fig. 5k**), relative to such parameters in mice reconstituted with B6.*Cd79a*$^{-/-}$ BM plus B6.WT BM. The onset of the immunological dysregulation was delayed in the mice reconstituted with B6.*Cd79a*$^{-/-}$ BM plus B6.Cav1KO BM relative to that in mice reconstituted with only Cav1-deficient BM (data not shown), which suggested that Cav1 deficiency in other immune cells, in addition to B cells, might aid in the development of the phenotype observed.

Defective central tolerance in B6.Cav1KO mice

Central B cell–tolerance checkpoints and peripheral B cell–tolerance checkpoints ensure the removal of autoreactive B cells in the BM and periphery, respectively[12]. To identify whether such checkpoints were defective in B6.Cav1KO mice, we purified immature B cells from the BM and splenic B cells and then cloned and sequenced transcripts from their productive *Igh* allele. The variable domains of B6.Cav1KO B cells carried longer complementarity-determining CDR3 segments harboring more positively charged amino acids than did such domains in their B6.WT counterparts (**Fig. 6a** and **Supplementary Fig. 6a**). Such features are a hallmark of autoreactivity[12]. Autoreactive immunoglobulin HCs were detected in immature B6.Cav1KO B cells from the BM (**Fig. 6a**), in support of the proposal of a defect in central tolerance. *Cav1* mRNA was significantly more abundant in immature B cells than in B cells at other developmental stages (**Fig. 6b**). B cell development in B6.Cav1KO BM was unaltered (relative to that in B6.WT BM), with two exceptions: first, a increase specifically in mature recirculating B cells (**Fig. 6c**), and second, a reduced proportion of cells expressing the λ-light chain (λLC) (10% reduction; **Supplementary Fig. 6b**). The frequency of transitional CD93$^+$ B cells in the spleen was lower and the proportion of anergic B cells was greater in B6.Cav1KO mice than in B6.WT mice (**Supplementary Fig. 6c**). Together these data supported the proposal of a break in central tolerance but partially functional peripheral tolerance, which would explain the development of features of autoimmunity rather late in life in Cav1-deficient mice.

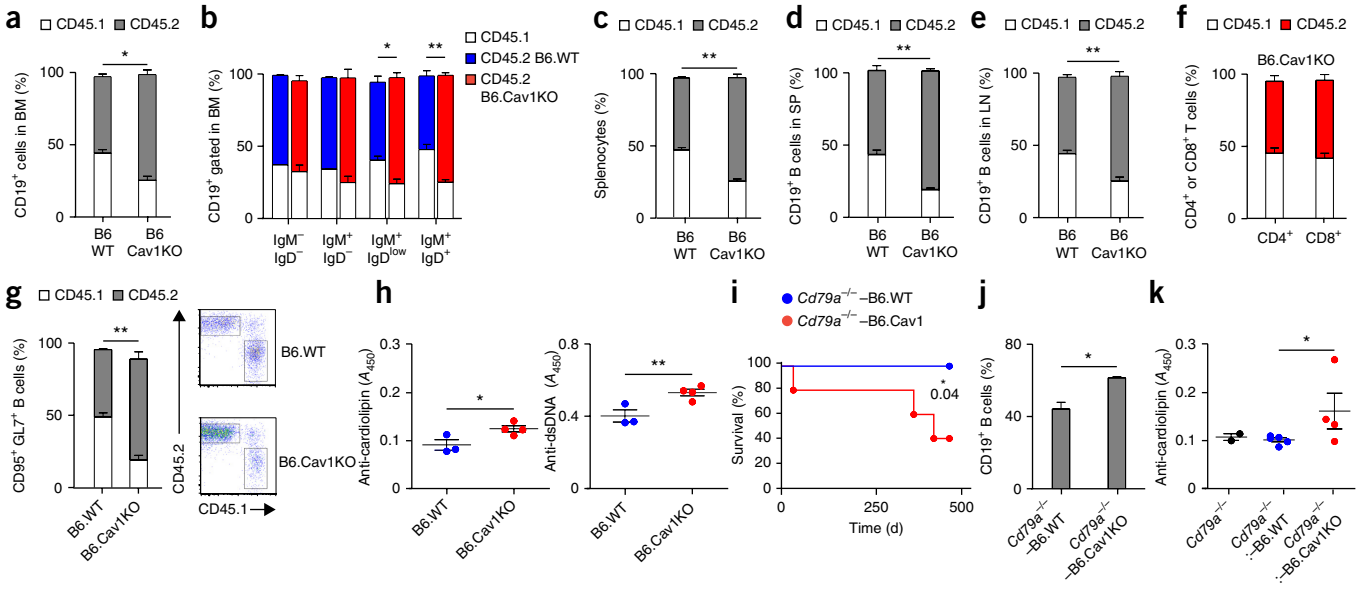

Figure 5 Cav1-deficient B cells have a competitive advantage in BM repopulation. (**a**) Frequency of wild-type CD45.1$^+$ or CD45.2$^+$ donor B cells (key; red and blue, as along horizontal axis) in the BM of sublethally irradiated *Rag2*$^{-/-}\gamma c^{-/-}$ host mice (n = 3–4 per group) at 24 weeks after injection of a mixture (1:1) of B6.CD45.1 BM cells plus B6.WT or B6.Cav1KO BM cells. (**b**) Average chimerism of gated CD19$^+$ B cells in the BM along B cell development in host mice as in **a**. (**c**) Frequency of CD45.1$^+$ and CD45.2$^+$ splenocytes in host mice as in **a** (n = 3–4 per group). (**e**,**f**) Average chimerism of gated CD19$^+$ B cells in the spleen (SP) (**d**) and lymph nodes (LN) (**e**) of host mice as in **a**. (**f**) Frequency of CD45.1$^+$ and CD45.2$^+$ cells among gated CD4$^+$ or CD8$^+$ T cells (horizontal axis) in host mice as in **a** (n = 4 per group). (**g**) Average chimerism (left) of splenic GC B cells in host mice as in **a** (n = 3–4 per group) gated as at right. (**h**) ELISA of anti-cardiolipin (left) or anti-dsDNA IgG (right) in the serum of host mice as in **a** (n = 3–4 per group), presented as absorbance at 450 nm (A_{450}). (**i**) Survival of sublethally irradiated *Rag2*$^{-/-}\gamma c^{-/-}$ mice up to 63 weeks after injection of a mixture (1:1) of B6.*Cd79a*$^{-/-}$ BM cells plus B6.WT BM cells (*Cd79a*$^{-/-}$–B6.WT) or B6.Cav1KO BM cells (*Cd79a*$^{-/-}$–B6.Cav1KO). *P* values, log-rank (Mantel-Cox) test. (**j**) Frequency of splenic CD19$^+$ B cells of host mice as in **i** (n = 4). (**k**) ELISA of anti-cardiolipin IgG in the serum of host mice as in **i** (n = 4 per group) at 45 weeks after transplantation, or from aged matched B6.*Cd79a*$^{-/-}$ mice (control). Each symbol (**h**,**k**) represents an individual mouse; small horizontal lines indicate the mean (± s.e.m.). $^*P \le 0.05$ and $^{**}P \le 0.01$ (Student's *t*-test (except where stated otherwise); presented as in **Fig. 1**). Data are representative of two experiments.

In immature B cells, newly generated BCRs are tested for autoreactivity by means of BCR signaling. We thus investigated whether Cav1 also regulates the nanoclustering of IgM-BCRs in immature B cells. The proximity of the IgM-BCR to GM1-enriched membranes increased after stimulation in immature B6.WT B cells but was impaired by the expression of the mutant Cav1 that cannot be phosphorylated (Cav1Y14F) or the absence of Cav1 (**Fig. 7a**). The immature B cell line WEHI-231 (called 'WEHI' here) has proven to be a useful model for the study of BCR-induced apoptosis and clonal deletion of immature B cells. WEHI cells barely express Cav1, as described for other lymphoid cell lines[26]. In a gain-of-function experiment, a vector containing an internal ribosomal entry site plus sequence encoding green fluorescent protein (GFP) and *Cav1* or a vector containing that internal ribosomal entry site plus sequence encoding GFP alone was expressed in WEHI cells. IgM-BCR and GM1-enriched membranes coalesced and BCR and Cav1 gained proximity upon activation only in the cells expressing Cav1 (**Supplementary Fig. 7a**,**b**). When WEHI cells were stimulated with anti-IgM, successfully transduced (GFP$^+$) cells expressing Cav1 underwent a stronger apoptosis response than that of their GFP$^-$ counterparts (**Supplementary Fig. 7c**). Our data suggested that by compromising reorganization and signaling via the IgM-BCR at the membrane, Cav1 deficiency affected the efficient removal of autoreactive immature B cells.

We next established an *in vitro* system that mimicked the encounter of an autoantigen with immature B cells. BM from B6.Cav1KO and B6.WT mice was cultivated under conditions in which B220$^+$IgM$^+$ immature B cells were present (**Supplementary Fig. 7d**). Next, the F(ab′)$_2$ fragment of anti-IgM was added to the BM cultures, to mimic autoantigen. The proportion of IgM-expressing cells and surface expression of IgM-BCR were reduced only for B6.WT cells, not for B6.Cav1KO cells (**Supplementary Fig. 7d**,**e**). After activation of immature B cells via the BCR, efficient receptor editing leads to an increased use of λLCs[38]. Immature B6.Cav1KO B cells failed to increase their λLC expression after being activated *in vitro* (**Fig. 7b**). Next, B6.Cav1KO mice were crossed with 3-83Igi mice, which express *Igh* and *Igk* loci targeted with genes that encode an autoreactive BCR composed of a 3-83Hi HC and a 3-83κi LC[39]. The 3-83 BCR is autoreactive on the H-2^b (B6) background. The proportion of λLC$^+$ B cells is the best indicator of receptor editing in this model, since pairing of a wild-type κLC with a 3-83Hi HC creates a high frequency of autoreactive receptors. Three groups of littermates were analyzed: mice expressing both the 3-83 HC and 3-83 LC (3-83Hi–3-83κi), mice expressing the 3-83 HC and a wild-type LC (3-83Hi–WT), and mice expressing a wild-type HC and the 3-83 LC (WT–3-83κi). The frequency of λLC$^+$ cells in WT–3-83κi mice was similar to that of non-transgenic mice (**Fig. 7c**,**d** and data not shown), which indicated that pairing of the endogenous HC with the 3-83κi LC did not create autoreactive receptors. Pairing of the 3-83Hi HC with the wild-type LC (83Hi–WT), in contrast, generated autoreactive receptors, as demonstrated by a significantly greater frequency of λLC$^+$ B cells in 83Hi–WT mice than in WT–3-83κi or non-transgenic mice (**Fig. 7c**,**d** and data not shown). The greatest frequency of λLC$^+$ cells was observed in 3-83Hi–3-83κi mice (**Fig. 7c**,**d**). The frequency of λLC$^+$ B cells was lower in Cav1-deficient (B6.Cav1KO) mice expressing the 3-83Hi–3-83κi or 3-83Hi–WT BCR than in their Cav1-sufficient (B6.WT) counterparts (**Fig. 7c**,**d**). Together our data support a model

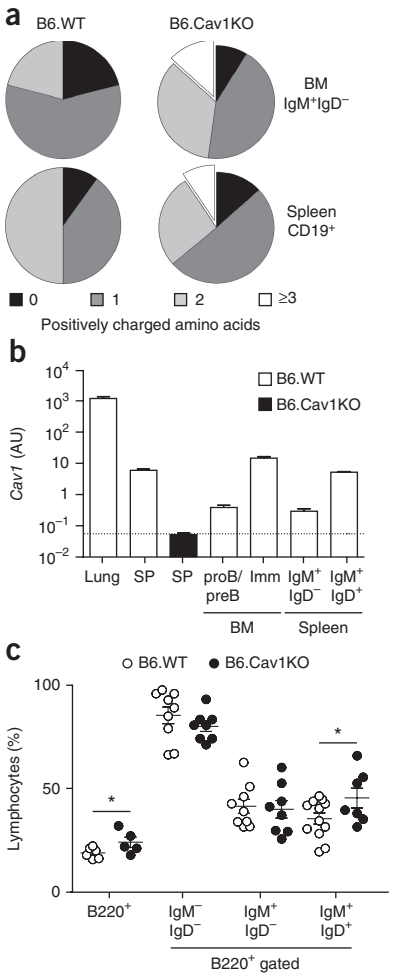

Figure 6 Cav1-deficient B cells express a skewed immunoglobulin HC repertoire. (**a**) PCR analysis of transcripts (128 sequences) from the productive, expressed *Igh* allele in B cell populations (right margin) sorted from the BM and spleen of 12-week-old B6.WT or B6.Cav1KO mice (above plots), followed by analysis with the sequence-analysis tool IgBLAST to identify positively charged amino acids (key). $P = 0.0029$ (Fischer's exact test). (**b**) Quantitative PCR analysis of *Cav1* transcripts in single-cell suspension of lungs, BM and spleen (SP), pro-B cells and pre-B cells (proB–preB) or immature B cells (Imm) sorted from the BM, or IgM$^+$IgD$^-$ or IgM$^+$IgD$^+$ B cells sorted from the spleen (below plot); results were normalized to those of the control gene *Gapdh* and are presented in arbitrary units (AU). (**c**) Flow cytometry of lymphocytes from 12- to 20-week-old B6.WT or B6.Cav1KO mice (key), assessing BM development (horizontal axis). Each symbol represents an individual mouse ($n = 5$–12 per genotype); small horizontal lines indicate the mean (± s.e.m.). *$P \leq 0.05$ (Student's *t*-test; presented as in **Fig. 1**). Data are representative of two experiments with two mice per genotype (**a**), two experiments with three pooled independent biological replicates (**b**; mean + s.e.m.) or five to twelve experiments with one mouse in each (**c**).

in which Cav1 regulates the nanoscale distribution of the BCR and thereby controls BCR activation. In immature B cells, defects in this distribution result in sub-optimal receptor editing, which leads to a break in B cell tolerance.

DISCUSSION

Our data have demonstrated that Cav1 regulated the following hallmarks of the nanoclustering of IgM-BCRs and IgD-BCRs on the surface of resting B cells: first, efficient exclusion of the IgM-BCR from GM1-enriched lipid domains; second, close proximity of the IgD-BCR to those lipids; and third, class-specific segregation of IgM-BCRs from IgD-BCRs. Thus, the previously described organization of the IgM-BCR and IgD-BCR protein islands or nanoclusters[16–18,20,34,40] requires Cav1. We have identified Cav1 as a molecular target that allows manipulation of the nanoscale organization of the B cell plasma membrane. Whether Cav1 orchestrates this basal compartmentalization during the sorting process at the Golgi apparatus or by scaffolding the IgD-BCR in GM1-enriched lipid domains, while excluding the IgM-BCR, remains to be investigated. Likewise, the motifs of the IgM-BCR and IgD-BCR that mediate this class-specific compartmentalization must be identified. Notably, cholesterol- and sphingolipid-rich domains exist in the absence of Cav1 in several cell types, including lymphocytic cell lines[26], and we showed here that the composition of these domains was not altered substantially in Cav1-deficient B cells. Therefore, it is very unlikely that our results were just a consequence of the lack of these domains in Cav1-deficient B cells. At steady state, nanoclustering of BCRs was regulated by phosphorylation of Cav1 at Tyr14. Cav1 is phosphorylated in resting B cells[41] and might recruit the Src kinase CSK[42] to mediate actin organization[43] and thereby prevent the diffusion of BCRs in the plasma membrane[20].

The stimulation of BCRs results in rapid coalescence of IgM-BCRs with GM1-enriched domains[44], diffusion of IgD-BCRs from those domains[18] and coalescence of nanoclusters of IgM and IgD[34]. Treatment of B cells with the F-actin inhibitor latrunculin A results in cell activation[20], which suggests that relaxing the actin cytoskeleton promotes diffusion in the membrane and the coalescence of BCR nanoclusters for signal propagation. Here we showed that all such translocations were impaired in the absence of Cav1, which suggests a connection among the BCR, Cav1 and actin reorganization after stimulation of the BCR. This connection might be mediated by the BCR-mediated recruitment of the phosphatase SHP2 to the membrane, which competes with CSK for binding to phosphorylated Cav1 (ref. 42). CSK is thus released from the membrane, and the actin cytoskeleton relaxes. Alternatively, localization of the ERM ('ezrin-radixin-moesin') family of actin-binding proteins to Cav1 and GM1-enriched domains[40] or the interaction of filamin A with Cav1 and actin[45] might mediate this connection. Ligand-induced redistribution of IgM-BCRs is sensitive to inhibition of the Src family of kinases by PP2 (ref. 46). Such data have been interpreted as an indication that the phosphorylation of BCR ITAMs drives this reorganization. Here we demonstrated that the Tyr14 in Cav1 contributed to translocation of the IgM-BCR into and the IgD-BCR out of GM1-enriched domains, which opens a discussion of how ligand-induced BCR signaling and the phosphorylation of Cav1 regulate the reorganization of BCRs. Our data have conclusively shown that in Cav1-deficient B cells, IgM-BCR and IgD-BCR islands failed to coalesce after activation and that BCR signaling was impaired but not fully abolished. In contrast, IgM-BCR and IgD-BCR domains coalesced in B6.Cav1$^{Y14F/Y14F}$ B cells, which showed a smaller reduction in activation than that of cells lacking Cav1 expression. Together these data suggest that the coalescence of IgM-BCRs and IgD-BCRs is a crucial step for efficient BCR signaling.

Despite their B cell dysfunction, aged B6.Cav1KO mice developed features of autoimmunity, such as spontaneous B cell activation, elevated autoantibody titers, a shorter lifespan and IgG deposits in the kidneys. Those hallmarks of autoimmunity were observed in two independent mouse models of Cav1 deficiency with different genetic backgrounds, as well as in BM-transfer experiments; this supports the proposal of their relevance. B cell–mediated autoimmunity has been

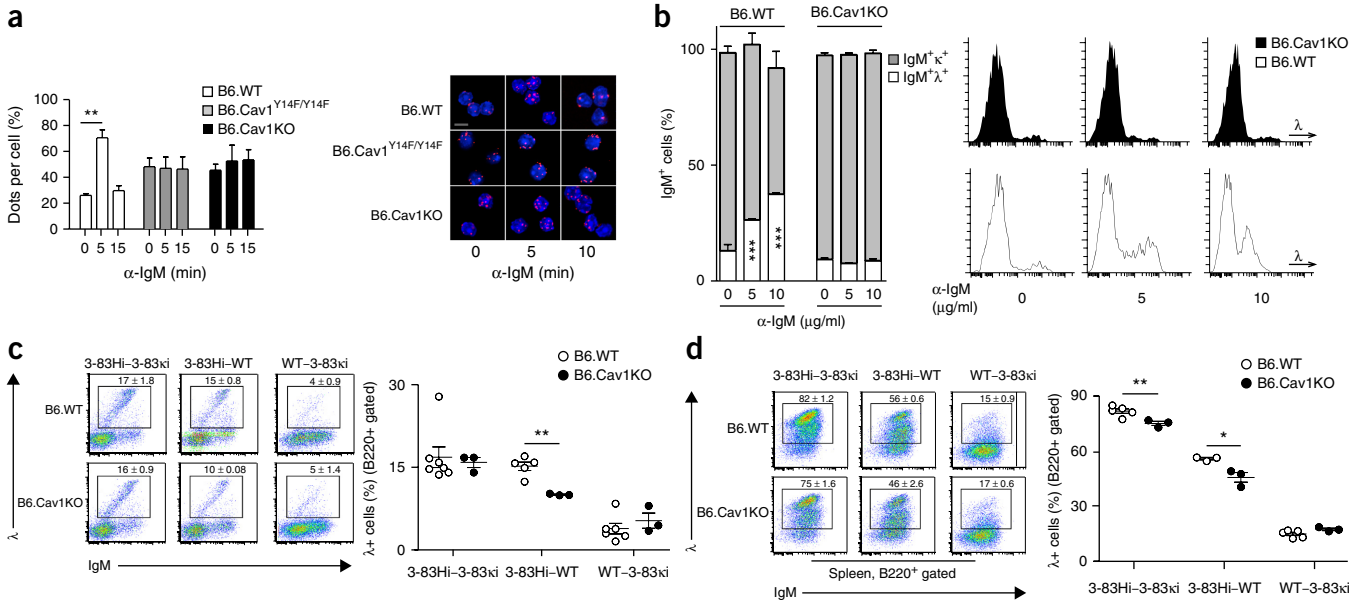

Figure 7 Defective receptor editing in B cells lacking Cav1 expression. (**a**) PLA (left) of unstimulated immature B cells (B220$^+$IgM$^+$IgD$^-$) purified from B6.WT B6.Cav1$^{Y14F/Y14F}$ or B6.Cav1KO mice (key) and allowed to 'rest' for 3–6 h in complete medium, then left unstimulated (0) or stimulated for 5 or 10 min (horizontal axis) with anti-IgM F(ab′)$_2$ (10 μg/ml) (assessed as in **Fig. 1a**); right, microscopy of cells as at left (as in **Fig. 1a**). Scale bar, 5 μm. (**b**) Frequency of IgM$^+$κ$^+$ or IgM$^+$λ$^+$ cells (key) among BM cells oftained from B6.WT or B6.Cav1KO mice ($n = 3$ per genotype) and grown *ex vivo* for 6 d in the presence of various concentrations (horizontal axis) of anti-IgM F(ab′)$_2$ (left), and flow cytometry identifying those cells (right). (**c**,**d**) Frequency of λLC$^+$ cells (indicative of receptor editing) in the BM (**c**) and spleen (**d**) of B6.WT and B6.Cav1KO mice (key) expressing the 3-83Hi–3-83κi, 3-83Hi–WT or WT–3-83κi HC–LC combination (horizontal axes) (right), assayed by flow cytometry of BM cells gated as B220$^+$, as at left. Numbers adjacent to outlined areas (left) indicate percent cells in each (mean ± s.e.m.). Each symbol (right) represents an individual mouse ($n = 3$–7 per genotype); small horizontal lines indicate the mean (± s.e.m.). $^*P \le 0.05$ and $^{**}P \le 0.01$ (Student's *t*-test; presented as in **Fig. 1**). Data are pooled from two to four independent experiments with at least 100 cells per condition in each (**a**) or 3 independent experiments (**b**–**d**; mean + s.e.m. in **b**).

associated with increased BCR signaling in the periphery or with a failure in the elimination of autoreactive B cells. Peripheral *Cav1*$^{-/-}$ B cells are not hyperactive. Therefore, Cav1 seems to be important for the efficient removal of autoreactive B cells, a conclusion supported by the skewed BCR repertoire and the presence of autoantibodies in Cav1-deficient mice. Autoreactive *Cav1*$^{-/-}$ B cells in the periphery might become activated by high concentrations of autoantigen and co-stimulatory signals from T cells and/or Toll-like receptors, which drive autoimmunity. Data obtained in human studies suggest that the threshold of BCR activation in the immature stages might define self-tolerance. For example, alterations in Lyn expression have been reported in patients with lupus[47]. Further, patients who carry mutations in the gene encoding the kinase Btk display a high frequency of autoreactive immature B cells[14]. Thus, Cav1-deficient mice emerge as a meaningful model showing that reduced BCR signaling can lead to autoreactivity and that recapitulates the self-reactivity associated with defects in BCR signaling observed in patients with common variable immunodeficiency or X-linked agammaglobulinemia.

The difference in the outcomes after activation of the IgM-BCR in immature B cells and mature B cells is not clearly understood. Studies using WEHI cells as a model of immature B cells have reported that the IgM-BCR fails to translocate to GM1-enriched domains after activation and have proposed that BCR signal initiation outside of those platforms in immature B cells activates a different cell-fate program: receptor editing or apoptosis[48]. However, we did not detect Cav1 expression in WEHI cells. After re-expression of Cav1, however, the IgM-BCR efficiently reorganized to GM1-enriched domains and enhanced IgM-induced apoptosis. Likewise, immature Cav1-deficient B cells failed to reorganize the IgM-BCR after stimulation or to initiate receptor editing by exchanging their LCs. Therefore, in both immature B cells and mature B cells, ligand-induced BCR reorganization is necessary for efficient signaling.

In summary, we have identified Cav1 as a regulator of the nanoscale organization of IgM-BCRs and IgD-BCRs in the plasma membrane of B cells. By targeting Cav1, we have demonstrated that nanoclustering of BCRs is crucial for setting the threshold of activation for both mature B cells and immature B cells. In immature B cells, the absence of Cav1 resulted in deficient counterselection of B cells expressing autoreactive BCRs, which ultimately led to autoimmunity in mice. This work underlines the emerging concept that immunodeficiency often manifests as autoimmunity, and will boost knowledge of diseases with dysregulation of the immune system.

METHODS

Methods, including statements of data availability and any associated accession codes and references, are available in the online version of the paper.

Note: Any Supplementary Information and Source Data files are available in the online version of the paper.

ACKNOWLEDGMENTS

We thank the BIOSS toolbox for reagents; M.C. Guadamillas and A. Cerezo for the generation of the B6.Cav1$^{Y14F/Y14F}$ mice; E. Hobeika (Max Planck Institute of Immunology and Epigenetics) for *Cd79a*$^{-/-}$ mice; H. Jumaa (Max Planck Institute of Immunology and Epigenetics) for 3-83Igi mice; C. Johner, U. Stauffer, N. Joswig, and K. Fehrenbach for experimental help; Y. Kulathu, M. Swamy M. Rizzi, K. Schachtrup and Y.R. Carrasco for critical reading of the manuscript; and W. Schamel for intellectual input and scientific discussions. Supported by the German Research Foundation (DFG) (SFB1160 IMPATH P5 to S.M., supporting F.A.H. and A.-M.S.; MI1942/2-1 to S.M., supporting G.J.F.; the Spemann Graduate School (Excellence Initiative GSC-4 to K.R.); the BIOSS Centre for Biological Signalling Studies (EXC294 to S.M. and M.R.); TRR130-P02 to M.R.; and

SFB746-P07 to M.R), the European Research Council (32297 to M.R.), the Spanish Ministry of Economy and Competitiveness (SAF2008-02100 (support for S.M. in 2008); SAF2011-25047, CSD2009-00016 and SAF2014-51876-R to M.A.D.P.; and support for CNIC), the Worldwide Cancer Research Foundation (15-0404 to M.A.D.P.), the Ramón y Cajal Program from the MINECO (2009-2011 to S.M.), Asociación Española Contra el Cáncer (I.N.-L.), the Pro-CNIC Foundation (support for CNIC) and Severo Ochoa Center of Excellence (SEV-2015-0505 for CNIC).

AUTHOR CONTRIBUTIONS

S.M. designed this study, performed experiments and wrote the manuscript with input from all authors; K.K. and A.-M.S. performed the PLA experiments; G.J.F. and F.A.H. performed *ex vivo* stimulation; T.O.-I. raised the mice and performed experiments; K.R. and M.S. performed kidney analysis; I.N.-L. performed DRM experiments; M.R. provided intellectual input and conceptual and scientific advice; M.A.D.P. provided B6.Cav1$^{Y14F/Y14F}$ mice, Cav1 expertise to the conception of the project and intellectual input and conceptual and scientific advice; and all authors critically read the manuscript.

COMPETING FINANCIAL INTERESTS

The authors declare no competing financial interests.

1. Hombach, J., Tsubata, T., Leclercq, L., Stappert, H. & Reth, M. Molecular components of the B-cell antigen receptor complex of the IgM class. *Nature* **338**, 760–762 (1990).
2. Reth, M. Antigen receptor tail clue. *Nature* **338**, 383–384 (1989).
3. Kurosaki, T. Genetic analysis of B cell antigen receptor signaling. *Annu. Rev. Immunol.* **17**, 555–592 (1999).
4. Rolli, V. *et al.* Amplification of B cell antigen receptor signaling by a Syk/ITAM positive feedback loop. *Mol. Cell* **10**, 1057–1069 (2002).
5. Meffre, E., Casellas, R. & Nussenzweig, M.C. Antibody regulation of B cell development. *Nat. Immunol.* **1**, 379–385 (2000).
6. Tonegawa, S. Somatic generation of antibody diversity. *Nature* **302**, 575–581 (1983).
7. Bassing, C.H., Swat, W. & Alt, F.W. The mechanism and regulation of chromosomal V(D)J recombination. *Cell* **109** (Suppl.), S45–S55 (2002).
8. Gu, H., Tarlinton, D., Müller, W., Rajewsky, K. & Förster, I. Most peripheral B cells in mice are ligand selected. *J. Exp. Med.* **173**, 1357–1371 (1991).
9. Shlomchik, M.J. Sites and stages of autoreactive B cell activation and regulation. *Immunity* **28**, 18–28 (2008).
10. Retter, M.W. & Nemazee, D. Receptor editing occurs frequently during normal B cell development. *J. Exp. Med.* **188**, 1231–1238 (1998).
11. Casellas, R. *et al.* Contribution of receptor editing to the antibody repertoire. *Science* **291**, 1541–1544 (2001).
12. Wardemann, H. *et al.* Predominant autoantibody production by early human B cell precursors. *Science* **301**, 1374–1377 (2003).
13. Menard, L. *et al.* The PTPN22 allele encoding an R620W variant interferes with the removal of developing autoreactive B cells in humans. *J. Clin. Invest.* **121**, 3635–3644 (2011).
14. Ng, Y.S., Wardemann, H., Chelnis, J., Cunningham-Rundles, C. & Meffre, E. Bruton's tyrosine kinase is essential for human B cell tolerance. *J. Exp. Med.* **200**, 927–934 (2004).
15. Grimaldi, C.M., Hicks, R. & Diamond, B. B cell selection and susceptibility to autoimmunity. *J. Immunol.* **174**, 1775–1781 (2005).
16. Schamel, W.W.A. & Reth, M. Monomeric and oligomeric complexes of the B cell antigen receptor. *Immunity* **13**, 5–14 (2000).
17. Yang, J. & Reth, M. Oligomeric organization of the B-cell antigen receptor on resting cells. *Nature* **467**, 465–469 (2010).
18. Kläsener, K., Maity, P.C., Hobeika, E., Yang, J. & Reth, M. B cell activation involves nanoscale receptor reorganizations and inside-out signaling by Syk. *eLife* **3**, e02069 (2014).
19. Maity, P.C., Yang, J., Klaesener, K. & Reth, M. The nanoscale organization of the B lymphocyte membrane. *BBA - Mol. Cell Res.* **1853**, 830–840 (2015).
20. Mattila, P.K. *et al.* The actin and tetraspanin networks organize receptor nanoclusters to regulate B cell receptor-mediated signaling. *Immunity* **38**, 461–474 (2013).
21. Parton, R.G. & del Pozo, M.A. Caveolae as plasma membrane sensors, protectors and organizers. *Nat. Rev. Mol. Cell Biol.* **14**, 98–112 (2013).
22. Goetz, J.G. *et al.* Biomechanical remodeling of the microenvironment by stromal caveolin-1 favors tumor invasion and metastasis. *Cell* **146**, 148–163 (2011).
23. Gaus, K., Le Lay, S., Balasubramanian, N. & Schwartz, M.A. Integrin-mediated adhesion regulates membrane order. *J. Cell Biol.* **174**, 725–734 (2006).
24. Hernández-Deviez, D.J. *et al.* Caveolin regulates endocytosis of the muscle repair protein, dysferlin. *J. Biol. Chem.* **283**, 6476–6488 (2008).
25. Hoffmann, C. *et al.* Caveolin limits membrane microdomain mobility and integrin-mediated uptake of fibronectin-binding pathogens. *J. Cell Sci.* **123**, 4280–4291 (2010).
26. Fra, A.M., Williamson, E., Simons, K. & Parton, R.G. Detergent-insoluble glycolipid microdomains in lymphocytes in the absence of caveolae. *J. Biol. Chem.* **269**, 30745–30748 (1994).
27. Tomassian, T. *et al.* Caveolin-1 orchestrates TCR synaptic polarity, signal specificity, and function in CD8 T cells. *J. Immunol.* **187**, 2993–3002 (2011).
28. Schönle, A. *et al.* Caveolin-1 regulates TCR signal strength and regulatory T-cell differentiation into alloreactive T cells. *Blood* **127**, 1930–1939 (2016).
29. Medina, F.A., Williams, T.M., Sotgia, F., Tanowitz, H.B. & Lisanti, M.P. A novel role for caveolin-1 in B lymphocyte function and the development of thymus-independent immune responses. *Cell Cycle* **5**, 1865–1871 (2006).
30. Drab, M. *et al.* Loss of caveolae, vascular dysfunction, and pulmonary defects in caveolin-1 gene-disrupted mice. *Science* **293**, 2449–2452 (2001).
31. Kenworthy, A.K., Petranova, N. & Edidin, M. High-resolution FRET microscopy of cholera toxin B-subunit and GPI-anchored proteins in cell plasma membranes. *Mol. Biol. Cell* **11**, 1645–1655 (2000).
32. Schmitz, R., Baumann, G. & Gram, H. Catalytic specificity of phosphotyrosine kinases Blk, Lyn, c-Src and Syk as assessed by phage display. *J. Mol. Biol.* **260**, 664–677 (1996).
33. Cao, H., Courchesne, W.E. & Mastick, C.C. A phosphotyrosine-dependent protein interaction screen reveals a role for phosphorylation of caveolin-1 on tyrosine 14: recruitment of C-terminal Src kinase. *J. Biol. Chem.* **277**, 8771–8774 (2002).
34. Maity, P.C. *et al.* B cell antigen receptors of the IgM and IgD classes are clustered in different protein islands that are altered during B cell activation. *Sci. Signal.* **8**, ra93 (2015).
35. Lee, W.-Y. & Tolar, P. Activation of the B cell receptor leads to increased membrane proximity of the Igα cytoplasmic domain. *PLoS One* **8**, e79148 (2013).
36. Razani, B. *et al.* Caveolin-1 null mice are viable but show evidence of hyperproliferative and vascular abnormalities. *J. Biol. Chem.* **276**, 38121–38138 (2001).
37. Park, D.S. *et al.* Caveolin-1 null (–/–) mice show dramatic reductions in life span. *Biochemistry* **42**, 15124–15131 (2003).
38. Gay, D., Saunders, T., Camper, S. & Weigert, M. Receptor editing: an approach by autoreactive B cells to escape tolerance. *J. Exp. Med.* **177**, 999–1008 (1993).
39. Pelanda, R. *et al.* Receptor editing in a transgenic mouse model: site, efficiency, and role in B cell tolerance and antibody diversification. *Immunity* **7**, 765–775 (1997).
40. Treanor, B., Depoil, D., Bruckbauer, A. & Batista, F.D. Dynamic cortical actin remodeling by ERM proteins controls BCR microcluster organization and integrity. *J. Exp. Med.* **208**, 1055–1068 (2011).
41. Vargas, L. *et al.* Functional interaction of caveolin-1 with Bruton's tyrosine kinase and Bmx. *J. Biol. Chem.* **277**, 9351–9357 (2002).
42. Jo, A. *et al.* SHP-2 binds to caveolin-1 and regulates Src activity via competitive inhibition of CSK in response to H2O2 in astrocytes. *PLoS One* **9**, e91582 (2014).
43. Radel, C. & Rizzo, V. Integrin mechanotransduction stimulates caveolin-1 phosphorylation and recruitment of Csk to mediate actin reorganization. *Am. J. Physiol. Heart Circ. Physiol.* **288**, H936–H945 (2005).
44. Gupta, N. & DeFranco, A.L. Lipid rafts and B cell signaling. *Semin. Cell Dev. Biol.* **18**, 616–626 (2007).
45. Muriel, O. *et al.* Phosphorylated filamin A regulates actin-linked caveolae dynamics. *J. Cell Sci.* **124**, 2763–2776 (2011).
46. Sohn, H.W., Tolar, P. & Pierce, S.K. Membrane heterogeneities in the formation of B cell receptor-Lyn kinase microclusters and the immune synapse. *J. Cell Biol.* **182**, 367–379 (2008).
47. Huck, S., Le Corre, R., Youinou, P. & Zouali, M. Expression of B cell receptor-associated signaling molecules in human lupus. *Autoimmunity* **33**, 213–224 (2001).
48. Sproul, T.W., Malapati, S., Kim, J. & Pierce, S.K. Cutting edge: B cell antigen receptor signaling occurs outside lipid rafts in immature B cells. *J. Immunol.* **165**, 6020–6023 (2000).

ONLINE METHODS

Cells and mice. The mouse B cell line K46 and its nitrophenol (NP)-specific mIgD-BCR- and mIgM-BCR-expressing transfectant line K46μmL was previously described[49]. K46μmL and WEHI-231 cells were cultured in RPMI-1640 complete medium supplemented with 10% FCS (FCS), 2 mM L-glutamine, 100 U/ml penicillin-streptomycin and 50 μM 2-mercaptoethanol and were grown at 37 °C in a humidified atmosphere with 5% CO_2.

The B6.Cav1KO mice[30], Cav1KO mice[36], 3-83Igi mice[39], B6.Cav1$^{Y14F/Y14F}$ mice[28], B6.*Cd79a*$^{-/-}$ mice[50], *Rag2*$^{-/-}\gamma c^{-/-}$ mice and B6.CD45.1 (C57BL/6 Ly5.1^{+}) mice were bred under specific pathogen-free conditions. Mice were sex matched and age matched with control littermates wherever possible. All animal protocols (G12/64) were performed according to the German animal protection law with permission from the responsible local authorities.

Flow cytometry. Organs were collected and processed to single-cell suspensions, and erythrocytes were removed by incubation in erythrocyte lysis buffer 150 mM NH_4Cl and 10 mM $KHCO_3$ for 4 min at about 20 °C. 0.3×10^6 to 0.5×10^6 cells were stained on ice and in the dark for 20 min in PBS containing 1% FCS and the appropriate antibodies (identified below). Before analysis, cells were washed a minimum of two times. Measurements were performed using a CyanTM (Beckham Coulter) or LSR II (BD Biosciences) flow cytometer and were analyzed with the FlowJo software.

Antibodies. The following antibodies were used for immunoblot analysis: anti-SYK (N-19; Santa Cruz), anti-IgM-HRP (Southern Biotech), anti-Cav1 (D46G3; Cell Signaling), anti-RAC1 (Millipore), anti-Lyn (Cell signaling) and anti-tubulin (Sigma).

The following antibodies were used for flow cytometry: anti-B220-PECy7 (RA3-6B2), anti-IgD (11-26), anti-IgM (polyclonal), anti-CD19 (1D3), anti-CD4 (GK1.5 and RM4-5), anti-CD8 (53-6.7), anti-CD93 (AA4.1), anti-CD69-PECy7 (H1.2F3), anti-CD86-PE (GL-1), anti-GL7, anti-CD95 (15A7) (all from eBioscience); anti-λLC λ1, λ2 & λ3 (R26–46), anti-κLC (187.1), anti-CD45.1 (A20), anti-IgD-FITC (11-26c.2a), anti-CD45.2 (105) and anti-Ki67 (B56) (all from BD Pharmingen); and anti-CD19 (6D5) (BioLegend). NP-BSA-biotin was from Biosearch Technologies. Anti-IgM-Fab-Alexa 647 was from Jackson ImmunoResearch (goat polyclonal antibody; 115-607-020). CFSE was from Sigma.

B cell purification and *in situ* PLA. For PLA, the following reagents were used: anti mouse-Cav1 (D46G3; Cell Signaling), antibody to mouse immunoglobulin α-chain (HM47/A9, BSA and azide free, Abcam), anti-mouse IgM (clone 1B4B1, Southern Biotech), anti-mouse IgD (clone 11-26c.2a, Southern Biotech) and CTxB (Sigma-Aldrich). F(ab′)$_2$ fragments were prepared of anti-IgM, anti-IgD and antibody to mouse immunoglobulin α-chain with a Pierce Fab Micro preparation kit (Thermo Scientific) using immobilized papain according to the manufacturer's protocol. After desalting (Zeba spin desalting columns, Thermo Scientific), the F(ab′)$_2$ fragments and CTxB were coupled with PLA Probemaker Plus or Minus oligonucleotides (Sigma-Aldrich) to generate PLA probes. Binding of anti-Cav1 was detected with oligo-coupled secondary anti rabbit antibody (DUO92002, Sigma-Aldrich). 'Untouched' B cells were purified from spleen using the MACS B cell isolation kit (Miltenyi Biotech). Purity was >90% as confirmed by flow cytometry using anti-CD19 (1D3, eBioscience). The PLA for the BCR and CTxB in non-permeabilized cells was previously described[18]. In brief, B cells were settled onto polytetrafluoroethylene slides (Thermo Fisher Scientific) for 30 min at 37 °C. BCR stimulation was performed with 5 μg/ml goat anti-mouse IgM F(ab′)$_2$ (1022-01, Southern Biotech), anti-mouse IgD F(ab′)$_2$ (2032-01, Southern Biotech) or 0.5 mM of pervandate. Pervanadate was freshly prepared for each experiment with equal molar amounts of orthovanadate and H_2O_2. For Src-kinase inhibition, cells were pre-treated with 10 μM PP2 (Sigma-Aldrich) for 60 min before the stimulation. Upon stimulation, cells were fixed with 4% PFA at about 20 °C for 20 min. For intracellular PLA, cells were permeabilized after fixation with 0.5% saponin (Sigma-Aldrich, S7900) in PBS for 30 min. After blocking for 30 min, the cells were incubated with appropriate PLA probes in PBS. PLA reactions were conducted according to the manufacturer's protocol (Duolink, Sigma). The resulting samples were directly mounted on slides with DAPI Fluoromount-G (SouthernBiotech) to visualize the PLA signals in relationship to the nuclei. To perform a PLA of Cav1 and the BCR, cells were first fixed and then permeabilized, and the PLA was performed between oligo-labeled F(ab′)$_2$ fragment of antibody to mouse immunoglobulin α-chain (HM57; ThermoScientific) and an oligo-labeled secondary antibody recognizing anti-Cav1 (D46G3; Cell Signaling). Microscope images were acquired with a Zeiss 780 Meta confocal microscope (Carl Zeiss). For each experiment, a minimum of 300 splenic cells or 100 immature cells were analyzed using the BlobFinder software and were validated using ImageJ. Blob size was defined as pixel size of 5 × 5. Raw data were exported to Prism software (GraphPad Software). For each sample, the mean PLA signal count per cell was calculated from the corresponding images. In all PLA experiments, the data were normalized to those of the pervanadate-stimulation condition to pool independently performed experiments, since the number of dot per cell varied between experiments. The PLA of IgM-BCR and IgD-BCR was performed as previously described[34].

Cell stimulation and protein purifications. Purified B cells were starved for 1 h and then were stimulated for various times at 37 °C with 10 μg/ml anti-mouse IgM F(ab′)$_2$ (115-006-075, Dianova) or with 0.5 mM pervanadate for 3 min. Treatment with the SRC family kinase inhibitor PP2 (Sigma) was performed at a concentration of 20 μM for 30 min at 37 °C before stimulation. RIPA buffer was used for cell lysis. Phosphorylated tyrosine was immunoprecipitated with 4G10-Sepharose (Sigma). Lipid-ordered detergent-resistant membranes (DRMs) were prepared as previously described[51].

***Ex vivo* stimulation and Ca^{2+} flux.** For *ex vivo* stimulation, purified splenic B cells (0.2×10^6 per sample) were maintained in RPMI containing 10% FCS, 2 mM L-glutamine, 100 U/ml penicillin-streptomycin and 50 μM 2-mercaptoethanol at 37 °C in a humidified atmosphere with 5% CO_2, and incubated with the appropriate stimuli for 18 h before being stained with anti-CD19-PB (6D5, BioLegend) and anti-CD69-PECy7 (H1.2F3, eBioscience), anti-IgM (1021-02, eBioscience) and anti-CD86-PE (GL-1, eBioscience).

For proliferation experiments, purified B cells (0.2×10^6 per sample) were labeled with CFSE in PBS containing 0.5% bovine serum albumin (BSA) according to the manufacturer's instructions (Invitrogen) for 10 min at 37 °C in the dark and 5 min on ice. After 3 d in culture with the appropriate stimuli (3 μg/ml anti-IgM F(ab′)$_2$ fragments (115-006-075, Dianova) or 1 μg/ml LPS (Sigma)) in the presence of 0.5 ng/ml IL-4 (Peprotech), cells were stained with PB-labeled anti-CD19 (6D5, BioLegend) and the CFSE fluorescence of the CD19^{+} cells was measured by flow cytometry.

For Ca^{2+}-flux analysis, B cells were labeled with 5 μg/ml Indo-1 and 0.5 μg/ml pluronic F-127 (both from Molecular Probes, Life Technologies) for 45 min in RPMI containing 1% FCS in the dark. Cells were washed and kept on ice until measurement. The baseline was recorded and cells stimulated with anti-IgM F(ab′)$_2$ (115-006-075, Dianova). The change in the ratio of Ca^{2+}-bound Indo-1 to Ca^{2+}-unbound Indo-1 was recorded with a LSRII fluorescence spectrometer (BD Biosciences). Data were analyzed with FlowJo software.

BM cultures and BM chimeras. BM cultures were prepared from freshly isolated BM cells following erythrocyte lysis. Cells were cultured in IMDM containing 10% FCS, 100 U/ml penicillin-streptomycin, 50 μM 2-mercaptoethanol and interleukin 7 (IL-7) at 37 °C with 7.5% CO_2 for 2 d. Then one half of the culture supernatant was removed and substituted by the same medium without IL-7. Survival and surface protein expression was analyzed by flow cytometry.

For BM chimeras, 'untouched' hematopoietic stem cells were purified using the MACS cell lineage depletion kit (Miltenyi Biotech) from freshly isolated BM cells, following erythrocyte lysis. Equal numbers of cells were injected into sublethally irradiated (400 rads) *Rag2*$^{-/-}\gamma c^{-/-}$ mice. After the appropriate time, the mice were killed and analyzed for reconstitution.

Immunization. To immunize mice, 4-hydroxy-3-nitrophenol conjugated to AECM-Ficoll (NP-Ficoll, Biosearch Technologies) was precipitated in alum by mixture (1 mg/ml) with an aluminum hydroxide solution at a ratio of 1:1. Precipitation in alum makes hapten-Ficoll a modestly stronger antigen[52]. Mice were immunized intraperitoneally with 376 μg per 100 g body weight. After 7 d, mice were killed and single-cell suspensions of the spleen were analyzed by flow cytometry and ELISPOT assay performed as previously described[53].

doi:10.1038/ni.3813

For the presence anti-NP, mice were immunized as described above and blood was collected every 7 d.

ELISA, repertoire analysis and quantitative RT-PCR. Quantification of total IgG antibodies and IgG autoantibodies recognizing dsDNA and cardiolipin was performed by ELISA as previously described[54] with minor modifications. In detail, eight serial dilutions were done, and the half maximal effective concentration (EC_{50}) was calculated for each mouse. The same approach was taken for the analysis of anti-NP after immunization. For repertoire analysis, total RNA was extracted from populations sorted from B6.WT or B6.Cav1KO mice. cDNA was prepared and *Igh* rearrangements were amplified by RT-PCR as described[55]. For qRT-PCR, total RNA of sorted populations was extracted and converted into cDNA. Mouse *Cav1* mRNA was quantified with SYBR green assay (Applied Biosystems). *Gapdh* amplification was used as a normalization control. The following primers were used:

Cav1 (forward) 5′-CAAGCATCTCAACGACGACG-3′,
Cav1 (reversed) 5′-GCAATCACATCTTCAAAGTCAATCTT-3′,
Gapdh (forward) 5′-TGAAGCAGGCATCTGAGGG-3′ and
Gapdh (reverse) 5′-CGAAGGTGGAAGAGTGGGAG-3′.

Kidney analysis. 1.5-µm sections were cut from formalin-fixed paraffin-embedded kidneys and were placed on coated objective plates. Deparaffination was performed in xylol, followed by ethanol with increasing aqueous fractions. Heat-mediated epitope retrieval was performed in a steamer with Tris-HCl, pH 6.1, for 20 min. After avidin-biotin blocking (Dako) and blocking with 5% mouse serum (Jackson Immunoresearch), slides were incubated with the biotinylated anti-mouse of the K5005 kit and were stained with an alkaline-based red chromogen reaction from the same kit (Dako) according to the manufacturer's guidelines. Afterward, counterstaining was performed with hematoxylin and methenamine silver stain to highlight basement membranes and to effectively distinguish proteins that were pathologically deposited from proteins in the plasma. A protocol of blind assessment and analysis by a trained pathologist was applied.

Statistical analysis. GraphPad Prism was used for data analysis and arrangement. For comparison of two data sets, a two-tailed Student's *t*-test was used. For comparison of three or more data sets, one-way ANOVA followed by Dunnett's multiple comparisons post-test were performed. Details on sample size, experimental replicates and statistics are included in the figure legends.

A **Life Sciences Reporting Summary** for this paper is available.

Data availability statement. The data that support the findings of this study are available from the corresponding author upon reasonable request.

49. Kim, K.J., Kanellopoulos-Langevin, C., Merwin, R.M., Sachs, D.H. & Asofsky, R. Establishment and characterization of BALB/c lymphoma lines with B cell properties. *J. Immunol.* **122**, 549–554 (1979).
50. Hobeika, E. *et al.* Testing gene function early in the B cell lineage in mb1-cre mice. *Proc. Natl. Acad. Sci. USA* **103**, 13789–13794 (2006).
51. Navarro-Lérida, I. *et al.* A palmitoylation switch mechanism regulates Rac1 function and membrane organization. *EMBO J.* **31**, 534–551 (2012).
52. Seppälä, I.J. & Mäkelä, O. Adjuvant effect of bacterial LPS and/or alum precipitation in responses to polysaccharide and protein antigens. *Immunology* **53**, 827–836 (1984).
53. Fiala, G.J. *et al.* Kidins220/ARMS binds to the B cell antigen receptor and regulates B cell development and activation. *J. Exp. Med.* **212**, 1693–1708 (2015).
54. Belver, L., de Yébenes, V.G. & Ramiro, A.R. MicroRNAs prevent the generation of autoreactive antibodies. *Immunity* **33**, 713–722 (2010).